THE USE OF MAGNETIC RESONANCE IMAGING AND PROTON SPECTROSCOPY TO IDENTIFY CRITICAL TISSUES IN DOGS WITH DUCHENNE MUSCULAR DYSTROPHY FOR FUTURE ASSESSMENT OF THERAPEUTIC INTERVENTION: A pilot study

---

A thesis
presented to
the Faculty of the Graduate School
at the University of Missouri-Columbia

In Partial Fulfillment
of the Requirements for the Degree
Master of Science

---

by

AMY ZALCMAN, DVM

Dr. Jimmy Lattimer, Thesis Supervisor

MAY 2018

The undersigned, appointed by the Dean of the Graduate School, have examined the thesis entitled

THE USE OF MAGNETIC RESONANCE IMAGING AND PROTON SPECTROSCOPY TO IDENTIFY CRITICAL TISSUES IN DOGS WITH DUCHENNE MUSCULAR DYSTROPHY FOR FUTURE ASSESSMENT OF THERAPEUTIC INTERVENTION: A pilot study

Presented by Amy Zalcman, DVM, a candidate for the degree of Master of Science and hereby certify that, in their opinion it is worthy of acceptance.

_____
Jimmy Lattimer, DVM, MS, DACVR, DACVR-RO

_____
Dongsheng Duan, Ph.D

_____
Craig Emter, Ph.D

_____
Stacey Leach, DVM, DACVIM-Cardiology

Dedication

This effort is dedicated to Isabella and Elliott Stewart who have been my constant companions throughout this endeavor. My eternal gratitude to my parents, Marilyn and Barry Zalcman.

ACKNOWLEDGMENTS

As most things of great value, this project was completed with a team effort. My sincere appreciation to James Holland, my partner in MRI, and Dr. John Dodam, my anesthesia guru. Drs. Jimmy Lattimer and Dongsheng Duan provided guidance and expertise at critical moments in the execution of this research. I am grateful for your insight and confidence in my abilities to execute this project. Dr. Richard Madsen who provided his expertise with statistics and woodworking. Chady Hakim and Gregory Jenkins contributed to the practical aspects of research and for that, I am sincerely grateful for their participation.

Table of Contents

List of Figures

List of Tables

List of Abbreviations

Term	Abbreviation
Duchenne Muscular Dystrophy	DMD
Dystrophin Associated Protein Complex	DAPC
Magnetic Resonance Imaging	MRI
Adenosine Triphosphate	ATP
Becker Muscular Dystrophy	BMD
Transforming Growth Factor	TGF
Picture Archiving and Communications Systems	PACS
Digital Information and COmmunication in Medicine	DICOM
Region of Interest	ROI
Intraventricular Septum	IVS
Left Ventricular Free Wall	LVFW
Papillary Muscle	PAP
False Discovery Rate	FDR
Average	AVG
Contrast	C

THE USE OF MAGNETIC RESONANCE IMAGING TO IDENTIFY CRITICAL TISSUES IN DOGS WITH DUCHENNE MUSCULAR DYSTROPHY FOR FUTURE ASSESSMENT OF THERAPEUTIC INTERVENTION

Amy Zalcman, DVM

Dr. Jimmy Lattimer, Thesis Supervisor

Abstract

Duchenne's Muscular Dystrophy is a debilitating disease that affects skeletal and cardiac muscle of 1 in 5000 male births. In the last thirty years, the gene responsible for the encoding of Dystrophin has been identified, sequenced and the variations of mutations described. There remains a void in the successful treatment of the disease although corticosteroid use has proven useful in delaying progression. Novel therapies are produced in the categories of virus-mediated gene delivery and stem cells, but evaluating their efficacy is hindered by an inability to contemporaneously assess the changes in muscle. The purpose of this pilot study was to characterize the changes in skeletal and cardiac muscle in a clinically advanced population of dogs affected with Duchenne Muscular Dystrophy. Using traditional sequences, delayed gadolinium enhancement, novel sequences and spectroscopy, changes in the investigated muscle were characterized. By establishing the differences between affected and unaffected dogs, the long-term goal of this body of work is to characterize these changes longitudinally and design a non-invasive method for tissue assessment as novel treatments are trialed.

1. Introduction

1.1 Duchenne Muscular Dystrophy- First observations

Duchenne Muscular Dystrophy (DMD) was first described in the *Annali Clinici dell'Ospedale degli Incurabili di Napoli* in 1836 by two Italian physicians, G.Coste and L. Gioja (1). There were several other case reports which culminated in the recognition of a familial "nature of the condition" by an English doctor, Edward Meryon in 1851 (1). Guillaume Duchenne devoted his medical career to obsessive observation and recording of the progression of this disease in one particular case. He documented changes in the tissue during various stages of disease to describe sequential pathology which he presented in a treatise in 1861 (1). Subsequently, Wilhelm Erb, a Bavarian neurologist, attempted to classify subtypes of muscular dystrophy in 1891 (1).

There was a large temporal gap until, in the 1940s, Peter Becker considered the pattern of distribution and thought it could be an inherited disorder (2). By 1955, Becker identified DMD as an as X-linked recessive disorder (3). It would be another thirty years, before the protein product was identified and then the gene locus was targeted. Yiu et al note that due to the large size of the gene and its abundance of exons (79), the gene is "susceptible to mutations, with one-third of mutations occurring *de novo*" (4).

1.2 The Dystrophin Molecule

The dystrophin protein is one of the largest proteins in the body, measuring 427 kDaltons. Its primary function is to link the internal cytoskeleton of a myocyte with the extracellular matrix. The composition of the protein is such that it maintains an amino terminus that binds to F actin and a carboxyl terminus that binds to the Dystrophin Associated Protein Complex (DAPC). The DAPC has constituent molecules: dystroglycans, sarcoglycans, integrins and calveolin.

Dystrophin is present in the myocytes of striated skeletal and cardiac muscles as well as the brain. In myocytes, the protein provides scaffolding for the fibrils. The DAPC is integral to the stability of actin and the sarcolemma within the fibril. This stability is critical to myocyte function over the lifetime of the individual and its absence results in catastrophic pathology.

1.3 From gene to fiber

A mutation in the dystrophin gene occurs in 1 in 5000 male births. Mutations in the 2.6 million base pairs tend to be large insertion or deletions; the remainder tends to be frameshift or point mutations. The end result is the inability to construct the protein (5). The absence of the dystrophin molecule initiates a chain reaction:

1. Destabilization of the DAPC
2. Diminished production of member proteins
3. Progressive fiber damage and membrane leakage
4. The myofibril is undermined with secondary influx of extracellular calcium

5. Protease activity results in myocyte death, necrosis and inflammation
6. Replacement by fibrosis

On a larger scale in skeletal muscle, the injury and inflammation are replaced by fatty infiltration.

1.4 Variations in the Myocardium

Ameen and Robson describe the altered pathology in the myocardium (6). In the absence of the dystrophin- glycoprotein complex, the sarcolemma is fragile and subject to shear trauma from contractions. This leads "to small tears in the cardiomyocyte membrane" as well as recently recognized dysfunction of the sarcolemmal stretch-activated ion channels (6). The inability of these ion channels to have coordinated function causes an influx of calcium into the cell and secondary calpains. Ameen notes that the protease function of the calpains degrade troponin and undermine the strength of mycocardial contractions (6). This promotes infiltration by inflammatory cells and fibroblasts (7). Like many myopathies, this results in increased wall stress and myocardial oxygen demand, which causes more cell death and fibrosis (7).

1.5 Making a diagnosis

There may be several features in the young person that may warrant pursuit of a diagnosis. If a family history prompts investigation, early creatine kinase elevations may raise suspicion. In the absence of a familial history, it may first present as a developmental delay (prior to

gait disturbance) (8). Mirski et al note that it is not uncommon to recognize symptoms in affected children prior to the age of 5 years in families without known risk (9). The group sites that affected children frequently have both cognitive and motor delays; the former is not widely associated with Duchenne Muscular Dystrophy (DMD). Mirski et al suggest that a component of delayed ability to walk may be due to this cognitive dysfunction (9).

Sussman describes the classic manifestation in an affected child who usually begins to walk between 18 to 24 months with a wide-based gait and stiff knees (2). Also in Stage I, calf muscle psuedohypertrophy is recognized by 3 to 4 years of age and changes in posture, like lordosis and wide-based stance, are noted as well. By the ages of 4 and 5 years, young boys cannot match their unaffected peers' athletic capabilities (2). More commonly recognized is the child's delayed ability to rise due to proximal limb weakness and are observed to use the Gowers maneuver. Gowers maneuver is comprised of a multistep process: the individual leans forward on their arms, elevates their pelvis with straight pelvic limbs, then straightens the thoracic extremities, and finally uses their core muscles to elevate to an upright posture.

Stage II is characterized by progressive deviation in the motor skills of affected boys from their peers (2). In this quiescent phase, boys cannot run, need assistance with climbing stairs and are generally weaker. Sussman describes that the wide-based stance is progressively wider, there is decreased heel contact during walking, and decreased knee flexion; the latter is common during the postural adjustments in weight acceptance when entering a standing position (2). Physical therapeutic intervention can help prevent complications from flexor contracture.

Near the beginning of the second decade of life, the ability to walk is compromised by profound proximal muscle weakness and core muscle fatigue. Stage III typically begins between 9 and 12 years; it is characterized by decreased ambulation and inability to rise from a sitting posture (2). Concomitant with decreased activity is weight gain which may further complicate motor function. Sussman notes that dietary counseling has not been helpful (2).

Complete loss of ambulation is a critical transition in affected individuals. It potentiates scoliosis and further impairs residual function. Stage IV, occurring between 12 and 16 years, is attributed to weakness in trunk and paraspinal muscles (2). Without surgical stabilization of the spine, the thorax eventually comes to rest atop the iliac crests. Early steroid intervention can retard some of this progression but it is associated with higher risk of vertebral fracture (8). Nocturnal ventilation is commonly introduced at this time (10).

Stage V is described by complete dependence and respiratory insufficiency. Sussman notes that patients maintain the capacity to chew and swallow soft foods but have lost nearly all limb function (2). Usually beginning by 15 years, this stage warrants complete respiratory support.

Bushby et al note that this timeline can be extended by integrated management of multiple medical services (8). With protraction of this timeline, cardiomyopathy has been more prevalent and more comprehensively described. Guglieri notes that up to 90% of affected individuals have cardiomyopathy by 18 years (11). Early and staged use of steroids can slow skeletal and cardiac muscle fibrosis (8). While this integrated approach has enabled

individuals to live into the later part of their fourth decade, it does not change the typical time point of loss of ambulation.

Clinical suspicions are confirmed with genetic testing and muscle biopsy with specific stains (12); in known risk families, this is typically performed early in life. Bushby et al describes that 10% of female carriers have clinical effects including heart and brain (8). Diagnostic methods have not evolved since 2010 (13). Papa et al evaluated a cohort of 15 pediatric carriers with unknown family history in which they recognized that 40% of this population showed muscle weakness by the end of infancy and 27% had behavioral issues (14). While the majority of carriers demonstrate symptoms at the time of puberty, cardiac failure is most common in late adulthood (15). A study, conducted in the Netherlands focusing on manifestations of heart disease in carriers, recognized that the mean age of carriers with diagnosed dilated cardiomyopathy was nearly 40 years (16). These changes were characterized by electrocardiogram and echocardiography.

The timeline of this disease in dogs is modified but the path of progression closely mimics people. For this reason, several colonies are maintained throughout the scientific community for use as a model of disease. Valentine et al describes that the first clinical recognition of disease is between 8 to 10 weeks if the animal survives the neonatal period; it demonstrates muscle weakness, stilted and short-strided/shuffling gait, and inability to open the jaw resulting in difficulty eating (17). Kyphosis progressing to lordosis, plantigrade stance and excessive drooling are commonly observed with progression (18) as well as restriction in the gait with earlier fatigue (19). Howell et al note that this is concomitant with hypertrophy of the tongue and temporal muscles secondary to dysphagia (19).

Cardiomyopathy is recognized at 6 months. The affected muscle groups in the colony described by Valentine et al include the tongue, diaphragm, antebrachial and crural extensors as well as muscle of shoulder flexion (17); this is known to vary between independent colonies.

1.6 Managing and Monitoring

DMD has a well-recognized timeline of progression that begins with gait abnormalities, progresses to core muscle weakness and scoliosis followed by progressive cardiomyopathy. Protective measures for decreased thoracic wall excursion include nocturnal ventilation. At present, daily steroid administration is the mainstay of therapy retarding pathology in skeletal and cardiac muscle. A large effort has been made in the area of gene replacement therapy which has produced optimistic, though short-lived, results. Many of the current gene therapies are comprised of micro or mini genes delivered via adenoviruses. These genes are available to the transcriptional mechanism of the cell which can produce a functional analog of the larger molecule, however, they are not incorporated to the larger genome. This requires repeated administration of the viruses which stimulate an immune response despite concomitant immunomodulatory therapy. Researchers have identified the need to modify the encapsulating virus to create the potential for repeated delivery. Monitoring patients with imaging has ranged from echocardiography and nuclear scintigraphy, to cross sectional imaging (computed tomography and magnetic resonance imaging).

In this project, magnetic resonance imaging is used to describe both the skeletal and cardiac muscle in a population of dogs with late-stage DMD. While this part of a grander effort to define the disease with MRI, it is important to understand the current applications of this modality in the disease. MRI has been employed in the characterization of this disease in excess of a decade. Initial description of the pathology has progressed to T2 mapping and spectroscopy. T2 mapping evaluates the subtle differences in signal intensity over a region of interest while spectroscopy is a non-invasive method to objectively assess the chemical composition of the muscle. A clinical correlation between spectroscopy and histopathology may negate future needs for invasive muscle biopsies. Consistently, MRI provides reliable spatial and contrast resolution over ultrasonographic techniques while decreasing operator-dependent variation in the exam (20).

1.7 Skeletal Muscle MRI

A characteristic pattern of muscular pathology is widely recognized in magnetic resonance imaging in patients with DMD. Thibaud et all describes changes in the magnetic resonance appearance of most muscles of affected dogs at all ages (21). The group sites changes in the forelimb muscles (flexors and extensors) as well as hindlimb muscles (gastrocnemius muscle bellies, superficial digital flexors and long digital extensor). Thibaud et al describes a more angular appearance, less subcutaneous fat and heterogenous signal distribution in dystrophic muscles in T2 weighted sequences (22). The group was able to demonstrate a quantitative difference in the T2 heterogeneity index and the maximal relative enhancement (22). In young boys, once the diagnosis of DMD has been made, it can be monitored non-invasively

with MRI in subclinical patients (23). In a range of studies, many approaches to DMD muscle characterization have been cultivated.

T1 Weighted Imaging

Initial attempts to describe changes focused on defining the T1 relaxation time of the affected versus non-affected subjects longitudinally. Quantitative analysis of DMD subjects was performed by Matsumura et al who demonstrated that T1 values initially increase then decline with progression of disease (24). This was attributed to progressive fatty infiltration (25). These changes were confirmed in canine DMD. Thibaud notes that the T1 relaxation time of affected canine muscle will change over time: in the first stage of disease, the T1 relaxation is prolonged while this shortens with progressive fat infiltration (22). T1 relaxation time can be correlated to signal intensity with standardized protocols.

T1 Weighted Imaging with Contrast

When administered, Gadolinium results in a local change in the magnetic field thus increasing the T1 signal (shortening T1 relaxation time) when present. This substance should remain extracellular when the muscle is healthy and the sarcolemma is intact. However, due to the accumulation of myocyte trauma with normal muscle use in patients with DMD, Gadolinium enhancement of affected muscles is marked (26). Post contrast images of muscles in dogs with DMD were more heterogeneous noting the importance of this component of the exam (22); they speculated that the interstitial volume is increased with degenerative changes and fibrosis. Thibaud discusses that both affected and normal muscle have delayed uptake and dissipation of contrast and attributes this to the relatively low perfusion during resting periods (22).

T2 Weighted Imaging

T2 weight sequences provide inherent contrast between hypointense muscle and hyperintense fat. Additionally, water and fluid create regions of hyperintensity within affected tissues. T2 relaxation times are prolonged in necrotic tissue, connective tissue or those displaying fat infiltration (27). In a group of young boys with DMD, Garrood et al demonstrated that the T2 values of all thigh muscles were higher than those of normal boys with the exception of the gracilis muscle (26). This is attributed to both inflammation and fat infiltration. Characterizing the skeletal muscles of dystrophic Golden Retriever Dogs, Thibaud et al identified more heterogeneity within the muscles of affected dogs, specifically the extensor carpi radialis brevis (22); they did not site a reasoning for this partiality.

In recent years, visual quantification of subtle variations in heterogenous tissue has been accomplished with T2 Mapping. T2 Mapping consists of establishing distribution of fat within muscle using T2 relaxation times. When performed in the calf muscles of affected individuals, there was a significant difference (28). Kim et al proposes this may be an "objective, quantitative method" to assess the disease over time demonstrating a spectrum of effect, siting that changes are most severe in the gluteus maximus and least severe in the gracilis (28). Although there is not a universally accepted reason for this disparity, it is attributed to the function of the muscles: the gluteus is required in the movement of the hip and thigh while the gracilis adducts the hip. The different functions reflect the demand on those muscles in early life and the subsequent accumulated trauma to myocytes during normal function.

Muscle volume

Mathur et al considered cross-sectional area of lower limb muscles in young men as a function of age (29). While there was an increase in cross-sectional area in the Duchenne population at all ages, they did not account for the proportion of fat infiltration in the muscle. This was not found to be a useful technique to monitor progression of the pathology.

Fat suppression

Using fat suppression techniques, fat signal intensity is strongly diminished. An increase in signal measured in muscle reflects the presence increased extracellular or unbound water content; this corresponds to edema or inflammation (25). In the early manifestations of DMD, this may provide more insight to the stage of muscle pathology.

Spectroscopy

Proton spectroscopy allows characterization of the chemical content of the sampled tissue. Both ^{1}H and ^{31}P have been used to characterize muscle in DMD. There is minute shielding of the magnetic field by adjacent atoms of a molecule (30). This produces a chemical shift of the resonant frequency that is measured in parts per million (ppm) and thus, certain molecules are characterized by specific peaks. Several lipids are represented in peak ranges 0.9, 1.1 and 1.3 ppm. The peak for choline, an abundant component of cell membranes, is observed at 3.2 ppm. Aisen et al describes the use of ^{31}P in cardiac muscle evaluation as it can be correlated to metabolism with molecules such as Adenosine Triphosphate (ATP) (30).

Lott et al conducted an evaluation of muscles of the lower limb with spectroscopy finding that lipid fractions were significantly elevated in DMD patients and that this change increases with advanced age (31). The group notes that the specific location of lipid within the muscle impacts the muscle function: intramyocellular lipid (within the cell, 1.3 ppm) and extramyocellular lipid (outside the muscle cell; 1.5 ppm) (31). In their protocol, they used both 1.5T and 3T magnets and did not report a difference in the quality of the spectra. When there is a large amount of fat infiltration in the tissue of interest, these peaks cannot always be separated. They acknowledge that the separation of these peaks was difficult to achieve in DMD patients but do not site whether this distinction is less apparent at earlier stages of disease.

Kinali et al demonstrated a good correlation between muscle biopsy and magnetic resonance imaging features for the extensor digitorum brevis in 10 of 15 patients (32). This is an ideal scenario to decrease the need for repeated muscle biopsy. Finanger et al sites that there is a limited amount of muscle mass and that processing biopsy samples create multiple opportunities for handling errors (25). She sites that this would be especially detrimental in clinical trials. In their evaluation of the forelimb, Thibaud et al acknowledges that the extensor carpi radialis and flexor carpi ulnaris were both visually most severely affected and convenient for measuring due to minimal error associated with slice averaging (22).

Elastography

Elastography is a novel method of investigating fibrosis with MRI. As of the preparation of this paper, the primary application is in the liver. It has not been routinely applied to other tissues "such as bronchial connective tissues, kidney, breast, skeletal muscle and brain" (33).

Ringleb et al characterized healthy muscle with MR elastography in 2007 however identify critical features that may hinder its application with patients affected by DMD (34). Typically, fibers need to be oriented in parallel directions which is unlikely to occur in clinically affected patients following the development of fibrosis (34). Additionally, the use of shear waves to induce the elastograph may cause further injury to the myocyte and hasten progression of disease.

1.8 Cardiac Imaging

Magnetic resonance has emerged as a critical tool in monitoring cardiac disease. Several methods of assessment have proven more sensitive and more accurate than echocardiography for functional and structural assessment. Dilated cardiomyopathy is now recognized as a common sequela of DMD since the introduction of improved management of respiratory manifestations (35). The subendocardial manifestations that occur in specific regions result in unique alterations in cardiac contractility (36). It is becoming a new focus for characterization of the disease. Myocardial fibrosis is correlated to left ventricular dysfunction and the resultant cardiomyopathy can culminate in heart failure (6).

The use of anesthesia in veterinary MRI complicates assessment of functional evaluation of with strain however, structural characterization is complete. Kornegay et al describes that "myocardial fibrosis and mineralization on pathologic evaluation" is observed as early as 6.5 months of age in affected dogs (18). With MR evaluation of the myocardium, they demonstrated that fibrosis is more pronounced in the left papillary muscle and apical ventricular free wall (18). Forder and Pohost recognize the challenge of successful

evaluation of the lipid content within the myocardium of the ventricular free wall in comparison to the interventricular septum due to pericardial fat (37). The contribution of fat may have to be indirectly evaluated as a subtraction technique between standard and fat-suppressed sequences.

T2 Weighted Imaging

In contrast to skeletal muscle, cardiac pathology is predominantly characterized by the deposition of fibrosis following an inflammatory phase. Excluding pericardial fat, there is a decrease in the inherent structural contrast in pathologic myocardium. Thus, gross assessment is not likely to identify subtle changes. "T2 relaxation time can be used to quantitate the tissue characteristics of the heart as it reflects the differences in water and fat content of the muscle" (6). This measurement will be able to impart earlier recognition of changes although it is not as sensitive as spectroscopy.

T1 Weighted Imaging with Contrast

In tissues that do not have inherent contrast in their natural structure, T1 weighted imaging with gadolinium contrast is a vital tool to describe the perfusion of a tissue when compared to the baseline T1 weighted images. As mentioned previously, gadolinium increases T1 relaxation time. Specifically, in regions of fibrosis, the structural changes that occur result in slower infusion of gadolinium and delayed wash out. Thibaud notes that the "late enhancement has been observed in dystrophic myocardium and has been correlated to fibrosis" (22). Silva et al also used delayed enhancement in the myocardium to describe myocardial fibrosis in boys with DMD and Becker Muscular Dystrophy (BMD) (35).

Ameen and Robson cite that fibrosis begins in the left ventricular free wall in patients with DMD while it is in the right ventricular free wall with BMD (6). It begins with the epicardium and progresses to the endocardium which they note is unique to dystrophic patients (6). Eventually, this ventricular chamber enlarges and the wall becomes thinner with further compromised contractility (6). In other cardiomyopathic diseases, thickening of the wall can also result in chronic ischemia of the endocardium. Kellman et al propose that the use of late enhancement paired with water and fat suppression sequences would permit this characterization of the myocardium (38).

Several studies have described the disproportionate progression of pathology in various regions of the myocardium. Although the pathophysiologic mechanism is unknown, the role of TGF-β (transforming growth factor) has a primary role in mediation of fibrosis in DMD and is suspected to contribute to this observation (39). Bilchick acknowledges that the regional differences in wall mechanics influences local gene expression as it relates to matrix remodeling and hypertrophy (39). Bilchick used late gadolinium enhancement to define specific distribution of scarring (fibrosis) in basal and mid-chamber locations and correlated this to strain analysis (39). This study described the inverse association between left ventricular ejection fraction and percent fibrosis. As a critical relationship, cardiac magnetic resonance earns its role in monitoring the progression of disease and success in treatment.

Black Blood

Black blood sequences exploit the regional magnetic susceptibility from altered states of iron in hemoglobin to reflect the local magnetic field. As a susceptibility weighted sequence, it sensitizes the traditional T2* to slow flow by applying a flow dephasing gradient to a 3D

gradient echo sequence (40). This improves the conspicuity of the endocardial margin and depresses the signal from fat. Kellman also used dark blood sequences to define pathologically thin-wall ventricles to improve ability to resolve the wall boundaries (38). In conjunction with the fat and water suppressed images, they suggest this will improve mapping of fibrofatty infiltration and distinguish this from normal epicardial fat. This technique employs a double inversion recovery sequence with improved signal to noise ratio that can enhance resolution with image reconstruction (38).

1.9 Treatment

The mainstay of treatment consists of corticosteroids introduced early in the disease process. Corticosteroids decrease necrosis and fatty infiltration in skeletal muscle to slow the progression of fibrosis; it has been the only medication to date that has successfully improved outcome (4). Pilot studies for nitroflurbiprofen, a nitric oxide releasing non-steroidal anti-inflammatory, have been completed in mice and subsequently, adults with DMD (41). An initial evaluation of 10 people is promising for the benefits of steroids (limiting inflammation and necrosis) without the side effects of muscle wasting. In mice, there exist a synergistic response with the use of nitric oxide as it increases the "bioavailability of nutrients [as well as] enhances the ability of myogenic stem cells to engraft to the dystrophic muscle" (41). Long-term use of this medication has not been evaluated (42).

Bushby et al note that steroid therapy is associated with a reduced risk of scoliosis although with a higher risk of vertebral fracture (8). The critical clinical point in DMD patient

progression is the development of scoliosis resulting from the reduced trunk and paraspinal muscle strength; this causes the predictable loss of ambulation. This has a direct correlation to respiratory compromise (8).

Steroids have also been shown to have a positive impact on the cardiac manifestations while non-steroidal anti-inflammatories have not yet been evaluated for this capacity. The early use of steroids has also been associated with improved cardiac function in later stages of the skeletal disease (7). Bilchick introduces the use of angiotensin receptor blockers, such as Losartan, to retard the progression of fibrosis in the myocardium (39). Specifically, this interferes with the TGF-β mediated pathway that promotes fibrosis.

The future in therapeutic interventions are diverse. Direct gene therapy promotes expression of a modified version of the dystrophin protein. Nowak et al reviews that direct injection of these therapies treats a small geographic area while systemic delivery has greater success to treat skeletal muscle which accounts for 20 percent body mass (5). Dudley et al showed 52% expression of dystrophin positive fibers concomitant with improved isometric force production one year after administration (43). Adenovirus mediated therapies, introducing a mini-dystrophin gene or component gene therapy, are finding early success advancing to Stage I clinical trials (44). Administered in immunosuppressed dogs, it can be given systemically for broader distribution (18). One of the greatest challenges is success in repeated doses since the immune system restricts efficacy of specific AAV strains. Myoblast transplantation has not been successful in people despite early success in mice; this has been attributed to "lack of cell survival, immune rejection and limited dispersal" (5). Stem cell use has been introduced and determined to be wide spread when administered systemically.

Ichim et al note that stem cells can fuse with dystrophic cells, have anti-inflammatory characteristics and produce factors which may function to promote endogenous repair (45).

Evaluation of these methods has been "impeded by a lack of sensitive, noninvasive, and objective outcomes" (46). Quantitative methods, such as spectroscopy may prove useful to this process. The aim of this study is to identify those tissues in mature adults that are markedly different than unaffected individuals. This effort is for the purpose of establishing a method of noninvasive monitoring to assess the efficacy of therapeutic interventions earlier in their use.

2. Materials and Methods

This is a prospective study in which all protocols were reviewed by the Institutional Animal Care and Use Committee at the University of Missouri. Six three-year-old purpose bred dogs from a colony of dogs with Duchenne Muscular Dystrophy were used. They were initially divided into Affected (n= 5) and Unaffected groups (n= 3). Affected dogs were identified at birth via genetic testing and muscle biopsy. One dog in the Unaffected group was later excluded as it was a Carrier; the latter group have a delayed and mild manifestation of pathology that is just now becoming characterized.

Table 1. List of dogs from which data is collected and presented here.

Name	**Age (years)**	**Gender**	**Affected/Unaffected**	**Genotype**
Patton	3	Male	Affected	GY
Philip	3	Male	Affected	GY
C-Lo	3	Male	Affected	GY
Aniya	3	Female	Affected	LW
Ariel	3	Female	Affected	LW
Tulip	3	Female	Carrier	XL
Griffin	3	Male	Unaffected	XY
Tony	3	Male	Unaffected	XY
Coke	3	Male	Unaffected	XY

Mutation: G= Golden Retriever; L= Labrador; W= Welsh Corgi

2.1 Anesthetic Protocol

Each dog was fasted from food since the evening before the day of the imaging exam. A physical exam was performed the morning of the anesthetic event by the Anesthesiologist (JRD) or the assisting veterinarian and vital parameters were recorded. Vital parameters include Weight, Heart rate, Respiratory rate, Rectal temperature and Capillary refill time.

Pre-anesthetic medication was comprised of an Intramuscular administration of dexmedetomidine (Orion, Finland; Domitor 0.5mg/mL) at a dose of 5 mcg/kg. Each dog was given between 10 and 15 minutes to reach effect during direct supervision. Dexmedetomidine was chosen as it could optimize the heart rate between 80 to 100 beats per minute in most dogs which is ideal for ECG gating. Additionally, it is known to be well tolerated by Affected dogs. Aseptic preparation of a cephalic vein immediately preceded placement of an intravenous catheter.

Anesthesia was induced and maintained with propofol (Novaplus, Lake Zurich, IL; Diprivan 10 mg/mL). The induction dose used was 6 mg/kg and an endotracheal tube was placed. Maintenance of anesthesia was achieved with a dose of 0.3 mg/kg/min via one of two methods. Calculated drip rate by the anesthesiologist (JRD) or a MRI compatible pump (Iradimed Corporation, Mridium 3861). Specifically, isoflurane gas anesthesia was avoided as it is known to cause sudden death during emergence in dogs with DMD; the exact mechanism is unknown.

Intravenous fluids were administered at a rate of 5 mL/kg/min; Lactated Ringers was used (Baxter Health Care, Deerfield, IL) was used. During the anesthetic period, oxygen was delivered by mechanical ventilation (Ohmeda, Madison, WI; Excel 210 MRI compatible) and temperature maintenance was encouraged with heat-trapping techniques. The ventilator was prepared with a 30-minute period of oxygen flush and then use of anesthetic gas scavenging filters (Dynasthetics, Salt Lake City; Vapor Clean).

Anesthetic monitoring consisted of several parameters using the Philips Invivo Expressions system (Orlando, FL). Heart rate, Respiratory rate, End Tidal CO2, ECG and Blood pressure were traced. ECG was monitored with an MRI- compatible thoracic-mounted pad and using an MRI compatible wireless tracer (989803163121**)** and presented with the video representation of the patient in the gantry (Philips, Expression IP5). SPO2 was monitored with a wireless tracer (989803163111).

Following image acquisition, a dedicated veterinarian recovered the individual while continuing to monitor Heart rate, Respiratory rate, and rectal temperature. Extubation was made after two robust swallow motions. The dog was continued to be observed for another minimum of 30 minutes prior to return to its housing unit. Food was offered upon return to the colony.

2.2 Diagnostic Imaging

Magnetic resonance imaging of the heart and skeletal muscle were performed before and after the administration of Gadodiamide (Novaplus, Omniscan, 287 mg/mL). Skeletal muscles of the pelvic limb (semimembranosus, gastrocnemius, and Sartorius) were imaged at the level of the stifle. The patient was placed in dorsal recumbency and physically supported in a lucite trough. At the level of the heart, a 16 channel, flexible transmit/receive coil (Toshiba, MJAJ-222A**)** was secured around the patient. A second coil (Toshiba, MJAJ-192A) was secured around the left stifle joint; it was a 4-channel flexible transmit/receive coil. Respiratory motion was diminished as gating with the mechanical ventilator was achieved easily. ECG gating was synchronized with the console. Imaging was made with a Toshiba 3T Titan Advantage at the Veterinary Health Center on the campus of the College of Veterinary Medicine at the University of Missouri. Gadodiamide (Novaplus, Omniscan, 287 mg/mL) was administered at a dose of 28.7 mg/kg in a rapid push; this was administered after the baseline T1 sequences of the cardiac muscle were made. Following the post Gadolinium sequence acquisition of the heart, the T1 post contrast sequences of the muscle were made.

Musculoskeletal Sequences

The following sequences and parameters were used to make the musculoskeletal images:

Table 2. List of sequences and parameters in musculoskeletal images

Weight	Plane	Type	TR (ms)	TE (ms)	FOV (cm)	Matrix	NAQ	Gating	Contrast
T2	SAG	FSE	5372	120	16 x 16	192 x 256	3	No	No
T2	AX	FSE	5372	120	16 x 16	192 x 256	3	No	No
T1	AX	FSE	723	10	16 x 16	192 x 208	1	No	No
Spectroscopy	Vol	FSE	3000	25	1.5x1.5 x1.7		128	No	No
T1	AX	FSE	723	10	16 x 16	192 x 208		No	Yes

Cardiac Imaging

The following sequences and parameters were used to make the cardiac images:

Table 3. List of sequences and parameters in cardiac images

Weight	Plane	Type	TR (ms)	TE (ms)	FOV	Matrix	NAQ	Gating	Contrast
2 Chamber Pseudo	SAG	FFE SSFP	3.4	1.7	28.5 x 28.5	192 x 192	1		No
HLA SSFP Cine	AX	FFE SSFP	3.4	1.7	23.8 x 23.8	160 x 160	1	ECG	No
SA Bright Blood	COR	FFE SSFP	3.4	1.7	23.8 x 28.5	160 x 192	1	ECG	No
T1 Black Blood	AX	FASE	1660	10	23.8 x 28.5	192 x 208	1	ECG and BH	No

T2 Black Blood	AX	FASE	1848	70	23.8 x 28.5	192 x 208	1	ECG and BH	No
T2 FS Black Blood	AX	FASE	1984	80	23.8 x 28.5	192 x 208	1	ECG and BH	No
SA 3D delayed FS	Short Axis	FFE3D	5.6	1.9	24.2 x 22.5	128 x 128	1	ECG and BH	No
SA 3D delayed FS	Short Axis	FFE3D	3.7	1.3	24.2 x 22.5	144 x 144	1	ECG and BH	No
SA 3D delayed FS	Short Axis	FFE3D	5.6	1.9	22.1 x 24.5	128 x 128	1	ECG and BH	Yes
SA 3D delayed FS	Short Axis	FFE3D	3.7	1.3	24.1 x 22.5	144 x 144	1	ECG and BH	Yes

BH= Breath Hold

2.3 Data Collection

Once the images were made and transferred to a Picture Archiving and Communication System (PACS) they were evaluated in a DICOM (Digital Information and COmmunication in Medicine) viewer, eFilm (Merge Health Care). Multiple measurements were made to describe muscle size and composition.

Musculoskeletal Values

Ratios

On the sagittal sequences, the ratio of the tibia to gastrocnemius muscle was made by measuring the tibia at the level of the proximal physeal scar and the gastrocnemius muscle at the same level (Figure 1). On the axial sequences, the ratio was made from the level of the largest cross-sectional area of the semimembranosus. The craniocaudal diameter of the distal femur is measured and compared to the craniomedial-caudolateral thickness (largest dimension) (Figure 2). All measurements of bone were made inclusively from the cortical margin to the other and measurements of the muscle were made at the longest length in the muscle, without obliquity, while perpendicularly to the axis of the muscle.

Figure 1. Musculoskeletal sagittal ratio

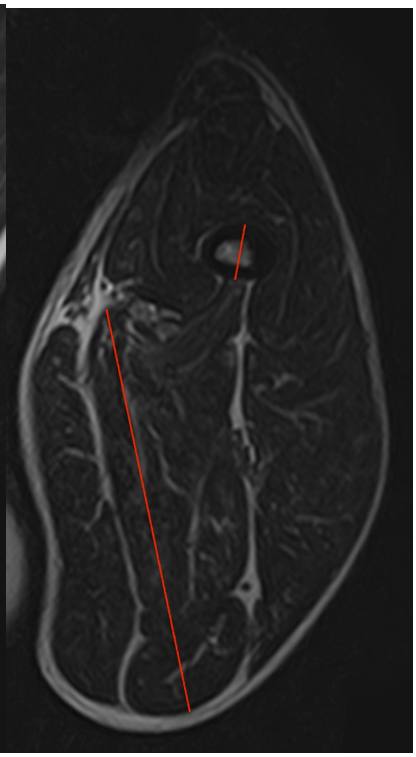

Figure 2. Musculoskeletal axial ratio

Signal Intensity

From the axial images of the T2, T1, and T1 Post contrast axial sequences, the signal intensity of several muscles were measured. At the same level as the ratio, signal intensity was measured by application of a region of interest (ROI) at three standardized locations in the semimembranosus muscles (1-3). Individual control ROIs were placed in the fat between the semimembranosus and semitendinosus (4), the marrow cavity of the femur (5), as well as the cranial and caudal muscle fascicles of the Sartorius muscle (6 and 7, respectively). (Figure 3).

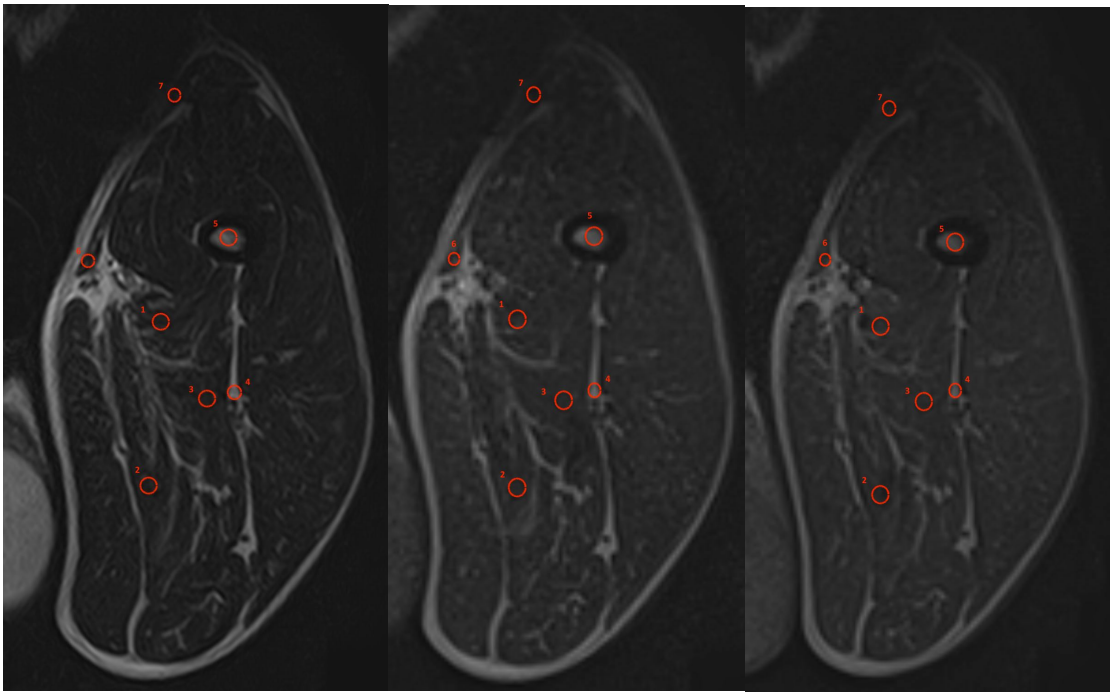

Figure 3. Signal intensity measurements in T2, T1, T1 + C

Spectroscopy

The values of the spectroscopy peak at 3.2 ppm, 1.3 ppm, 1.1 ppm, and 0.9 ppm were measured based on the size of the peak in comparison to the range on the y-axis (Figure 4).

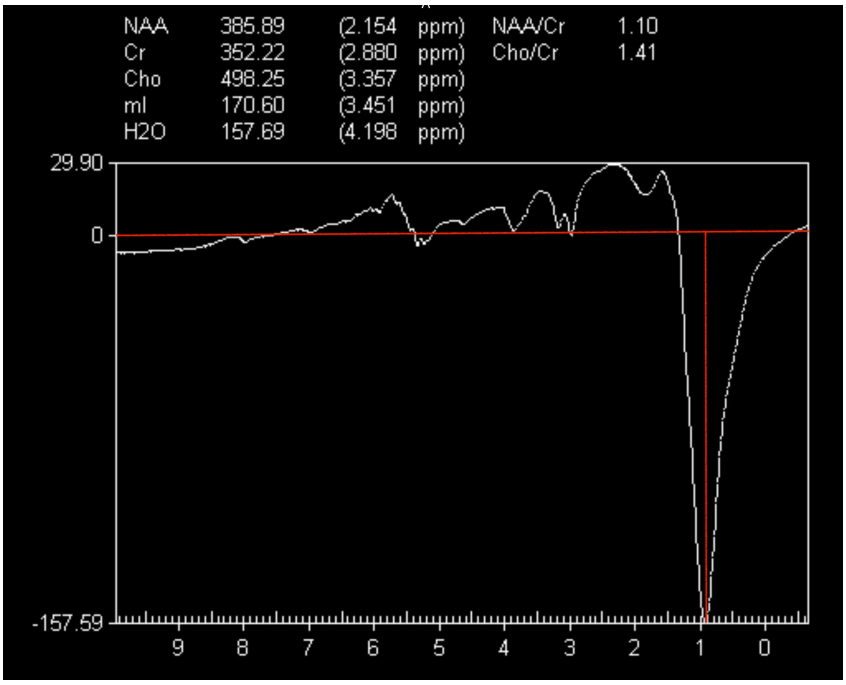

Figure 4. Musculoskeletal spectroscopy

Cardiac Values

Signal intensity

Several points of signal intensity were measured in the heart, using three areas in the liver as controls; the plane of the heart was at the level of papillary muscles. Figure 5 shows the plane of the heart where measurements were made.

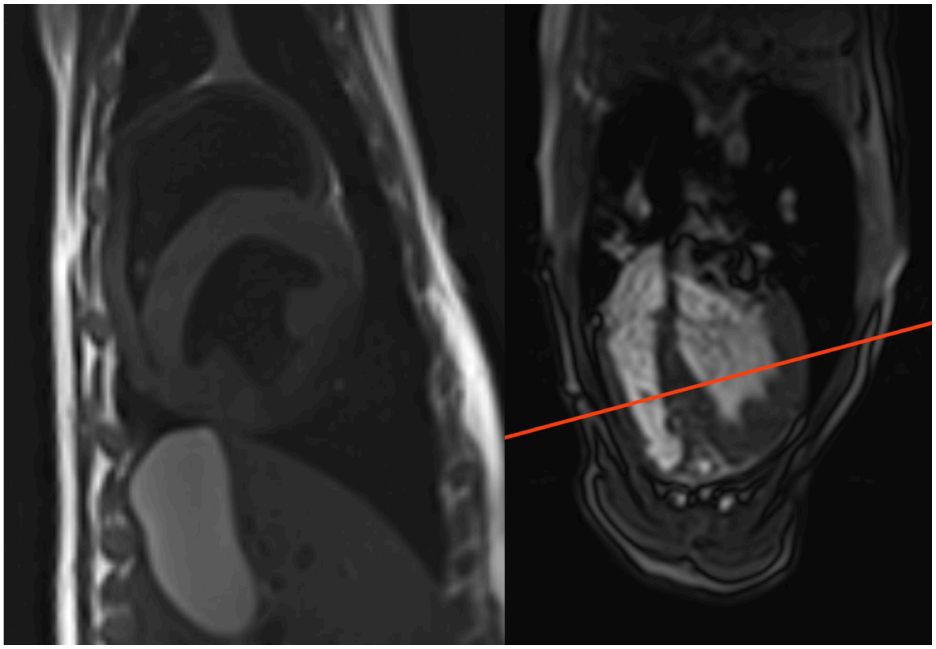

Figure 5. Plane of cardiac measurements

This was performed in the T2 Black blood, T2 Fat Saturated Black blood, T1 Black blood, and the Short Axis T1 3D Fat Saturated sequences (TE 1.3 and 1.9, both pre- and post-contrast). Three points were measured in the Interventricular Septum (IVS) and designated IVS-1, IVS-2 and IVS-3, respectively based on the caudal, middle and lateral thirds (Figure 6).

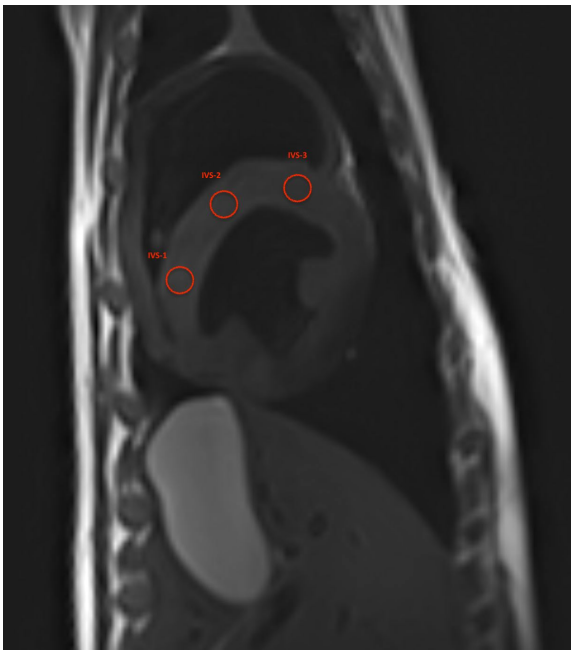

Figure 6. Cardiovascular signal intensity- IVS

Similarly, three points were identified along the Left Ventricular Free Wall (LVFW) and termed LVFW-1, LVFW-2, and LVFW-3 at the craniolateral, middle and caudolateral third, respectively (Figure 7).

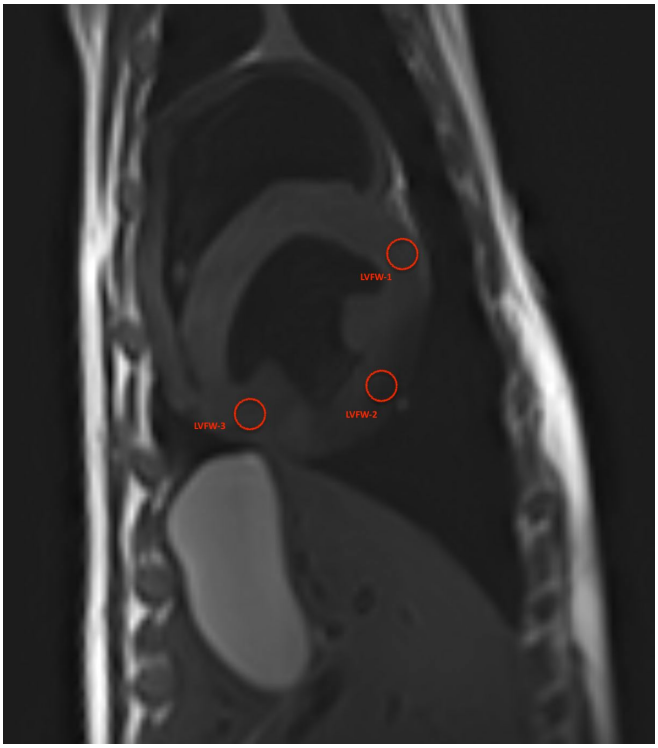

Figure 7. Cardiovascular signal intensity- LVFW

Signal intensity of the papillary muscles was collected for the posterior papillary (Pap-1) and anterior papillary (Pap-2) muscles (Figure 8).

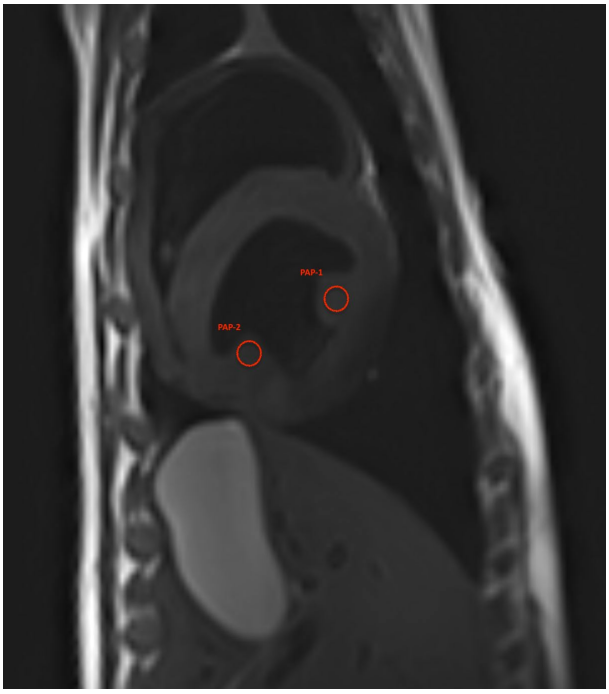

Figure 8. Cardiovascular signal intensity- PAP

Three locations in the liver were sampled. ROIs in the left, near center and the right liver were measured. The locations could not be standardized due to variations in gall bladder distention/position as well as phase of respiration (Figure 9).

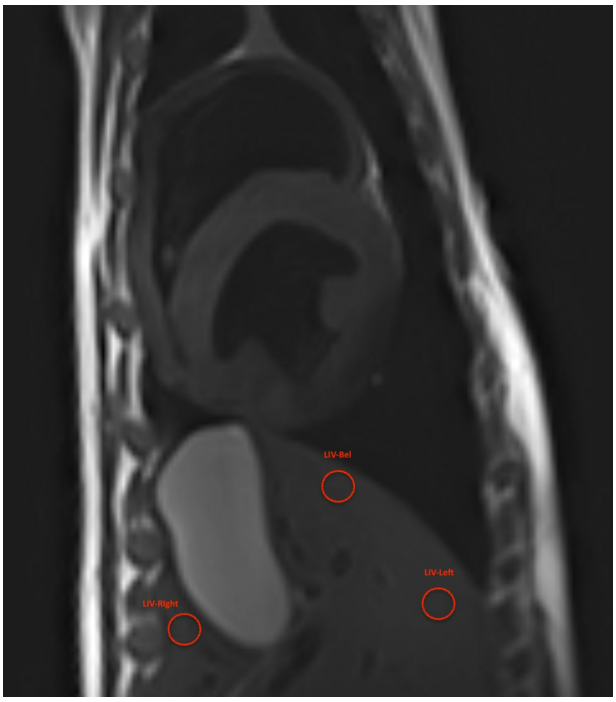

Figure 9. Cardiovascular signal intensity- Liver

2.4 Statistical Analysis

The data was evaluated with two-sample t-tests without assuming equal variances. Given the large number of tests, some adjustments were made for multiple testing and tests of hypotheses with some commonality were considered together. The p-values for a two-sided alternative were then adjusted for multiple testing by controlling the False Discovery Rate[1] at 0.05. Consequently, results reported here as significant have an FDR adjusted p-value less than 0.05. In addition to the tests of hypotheses, descriptive statistic including the mean, median, and standard deviation were found. Analyses were done using the statistical software SAS V9 (SAS Institute Inc., Cary, NC, USA).

[1] Benjamini, Y. and Hochberg, Y. (1995), "Controlling the False Discovery Rate: A Practical and Powerful Approach to Multiple Testing," ***Journal of the Royal Statistical Society, B***, 57, 289–300.

3. Results

Several different comparisons were made between the affected and unaffected dogs. A significance of level of 0.05 was used.

3.1 Musculoskeletal

The signal intensity of the affected semimembranosus muscle was compared with that of the unaffected semimembranosus muscle with the hypothesis that the signal intensity of the affected muscle would be higher in T2 weighted images than that of the unaffected muscle. There was not statistically significant evidence to reject the null hypotheses in this comparison.

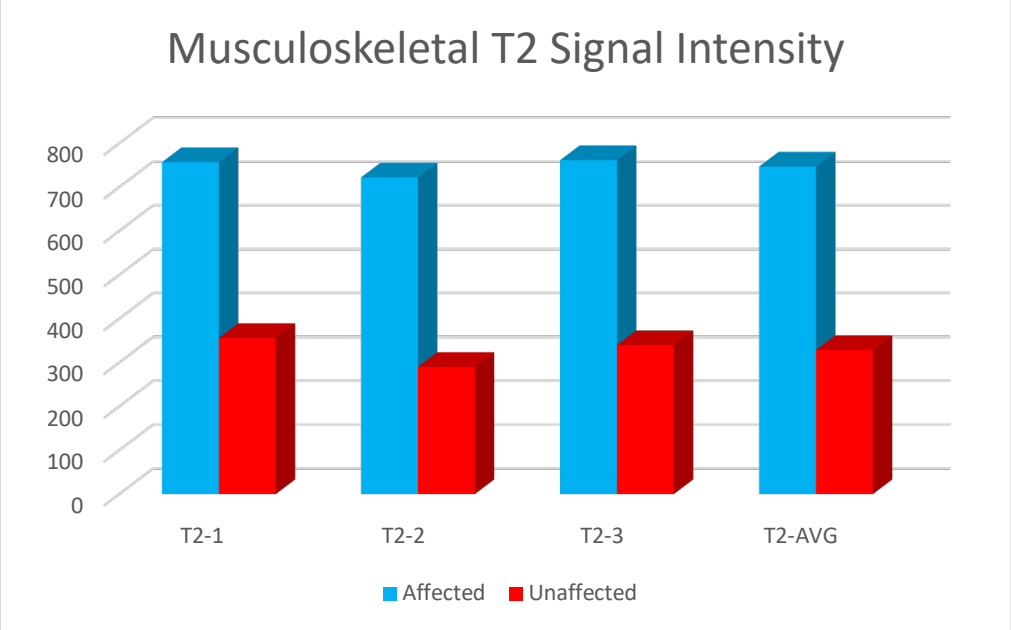

Figure 10. T2 Signal Intensity of the Semimembranosus Muscle

Table 4. Musculoskeletal T2 signal intensity

Site	Mean (Affected/Unaffected)	Standard Deviation (Affected/Unaffected)	Power (rounded to 0.00)
T2-1	756.9/356.0	356.0/53.5	0.123
T2-2	722.1/290.1	333.1/25.11	0.123
T2-3	761.4/339.6	447.5/53.0	0.123
T2-AVG	746.8/328.6	370.4/10.4	0.123

Additionally, the signal intensity of the semimembranosus was compared to both the cranial and caudal fascicles of the Sartorius, a muscle commonly spared in the human manifestations of DMD. The null hypothesis that there is no statistical difference between the variation of signal intensity between the semimembranosus and sartorial muscle of the affected and unaffected dogs. There was not statistically significant evidence to reject the null hypotheses in this comparison.

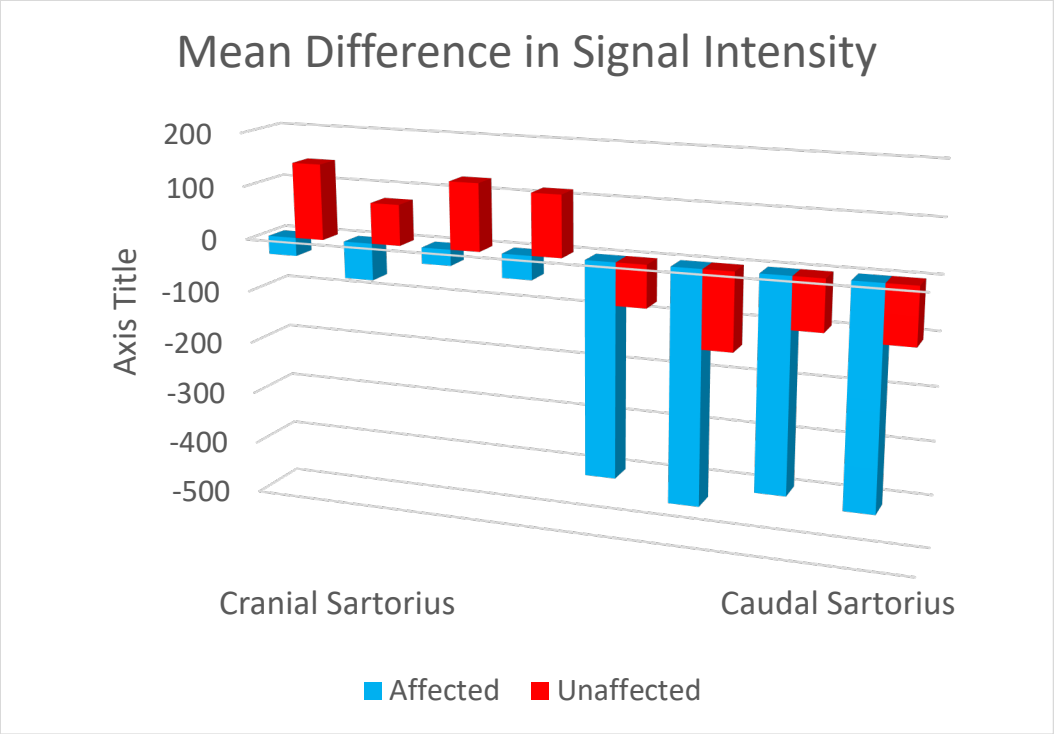

Figure 11. Comparison of Mean Differences between Affected and Unaffected with the Cranial and Caudal Bands of the Sartorius Muscle

Table 5. Musculoskeletal T2 signal intensity compared to Sartorius

Site	Mean Difference (Affected/Unaffected)	Standard Deviation (Affected/Unaffected)	Power (rounded to 0.00)
T2-1/ Cranial Sartorius	-34.7/142.2	511.3/80.8	0.659
T2-2/ Cranial Sartorius	-69.5/76.4	506.6/144.1	0.659
T2-3/ Cranial Sartorius	-30.2/125.9	548.1/175.0	0.659
T2-AVG/ Cranial Sartorius	-44.8/114.8	513.8/131.6	0.659
T2-1/ Caudal Sartorius	-402.7/-79.2	325.4/157.0	0.167
T2-2/ Caudal Sartorius	-437.5/-145.0	368.2/140.8	0.167
T2-3/ Caudal Sartorius	-398.2/-95.6	200.1/118.4	0.167
T2-AVG/ Caudal Sartorius	-412.8/-106.6	291.6/132.2	0.167

The muscle size was normalized to the size of the bone by establishing a ratio of the muscle to the bone. The bone size should have minimal variation between affected and unaffected animals and therefore provide an inherent measurement for standardization of the muscle size. On the sagittal sequences, this ratio was made at the level of the proximal tibial physeal scar to the thickness of the gastrocnemius muscle. On the axial images, this measurement was made across the femur in the cranial to caudal dimension at the level of the widest part of the Semimembranosus muscle; the latter measurement was used to calculate the ratio. The hypothesis tested entailed that there would be a difference between the muscle size of the affected and unaffected dogs. There was not statistically significant evidence to reject the null hypotheses in this comparison.

Table 6. Musculoskeletal Ratio

Ratio	Mean (Affected/Unaffected)	Standard Deviation (Affected/Unaffected)	Power (rounded to 0.00)
Sagittal	0.85/1.04	0.11/0.19	0.224
Axial	7.66/4.5 *	0.38/2.72	0.053

Table 7. Musculoskeletal axial ratio for affected and unaffected

*The following values are reported for the Axial ratio

Axial Ratio	Standard Deviation	Minimum/Maximum Values
Affected	0.375	7.27/8.11
Unaffected	2.72	1.88/7.23

Spectroscopy measurements were collected from discrete shifts in resonant frequencies that is measured in parts per million (ppm). Specific resonant frequency shifts were considered: 3.2, 1.3, 1.1, and 0.9 ppm. The peak at 3.2 represents choline which is a common component of cell membranes and is considered a correlation to the proportion of cells in the sampled volume. The peak at 1.3 corresponds to lipids; this value is if specific interest given the deposition of fat in described pathology of skeletal muscle death. Lactate also resonates at this peak and is a byproduct of anaerobic metabolism, a process that would be occurring at a higher rate in overtaxed skeletal muscle cells. Lipid peaks are also noted at 1.1 and 0.9. The alternative hypothesis would be a marked difference between the affected and unaffected dogs. It was anticipated that the lactate and lipid peaks of the affected animals would be have a larger peak value than those of the unaffected animals.

Table 8. Musculoskeletal spectroscopy

Peak (ppm)	Power (rounded to 0.00)
0.9	0.027
1.1	0.020
1.3	0.191
3.2	0.850

There was statistically significant evidence to reject the null hypothesis (0.9 ppm had a p= 0.027; 1.1 ppm had a p= 0.020). The spectral graphs of the affected (Figure 10) had a very distinctive appearance that contrasted sharply with the unaffected dogs (Figure 11).

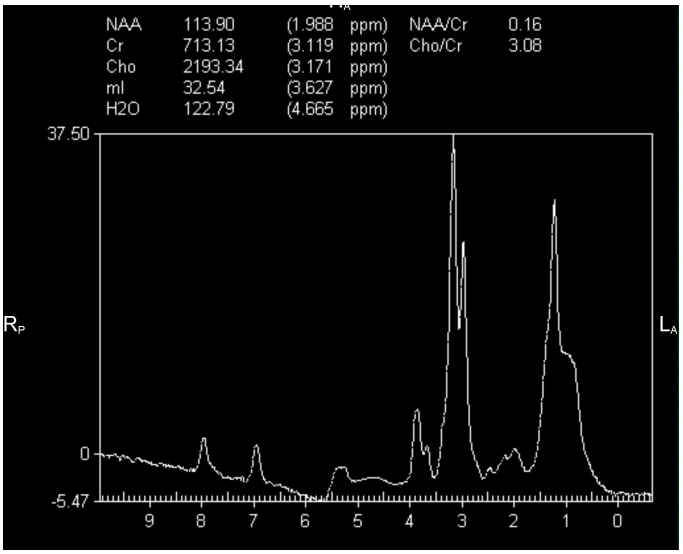

Figure 12. Normal musculoskeletal spectra

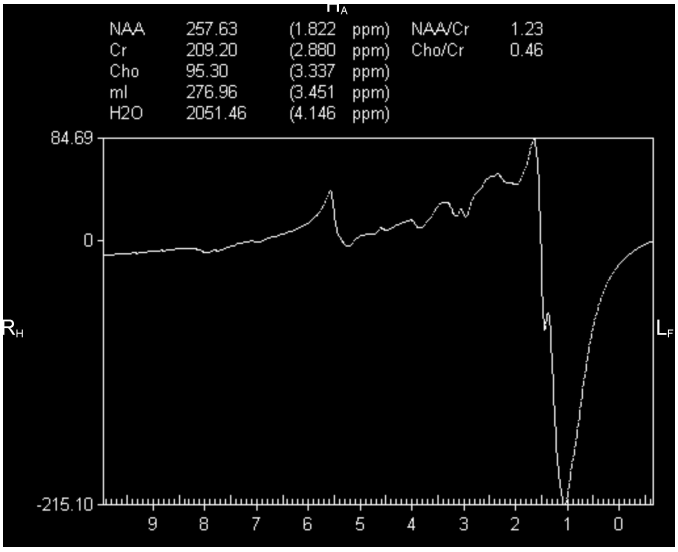

Figure 13. Affected musculoskeletal spectra

3.2 Cardiovascular

Many hypotheses were made regarding the signal intensity of the myocardium of the affected dogs in comparison to the unaffected dogs. This was performed for each location in the interventricular septum, the left ventricular free wall and the papillary muscles for each

sequence performed (T2, T1, T1 1.3, and T1 1.9). The null hypothesis in each situation was that the signal intensity of the affected myocardium is equal to that of the unaffected myocardium. The alternative hypothesis is that the signal intensity of the affected myocardium is not the same as the unaffected. Based on the disease pathology, the signal intensity of the affected muscle would be less than the affected. Following contrast administration, signal intensity of the affected myocardium would be higher.

The comparisons of the myocardium of the affected to unaffected dogs did not have statistical evidence to reject the null hypothesis for those signal intensities of the T2 weighted sequence.

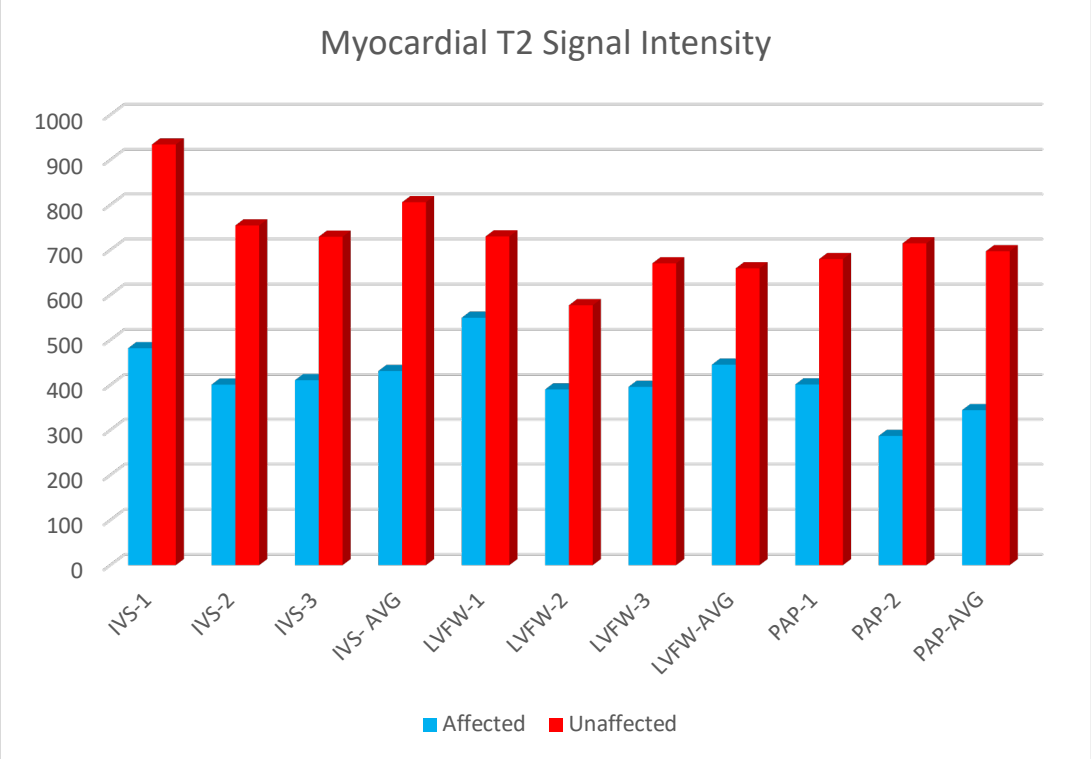

Figure 14. Graph of Myocardial T2 signal intensity values. Affected in blue, unaffected in red.

Table 9. Cardiovascular T2 signal intensity

Site	Mean (Affected/Unaffected)	Standard Deviation (Affected/Unaffected)	Power (rounded to 0.00)
IVS-1	481.9/934.4	185.1/44.1	0.118
IVS-2	400.96/754.6	144.8/200.6	0.118
IVS-3	410.8/729.5	256.8/384.5	0.143
IVS- AVG	431.3/806.2	402.0/193.5	0.118
LVFW-1	549.6/730.13	368.4/122.4	0.303
LVFW-2	390.3/577.37	173.3/212.4	0.303
LVFW-3	396.1/670.4	109.4/561.6	0.172
LVFW-AVG	445.35/659.3	179.2/298.8	0.275
PAP-1	401.4/679.8	161.4/115.6	0.172
PAP-2	287.1/714.8	144.9/308.6	0.118
PAP-AVG	344.3/697.3	149.3/191.0	0.118

For the T1 weighted sequences, there was sufficient statistical evidence to reject the null hypotheses for those measured points of the interventricular septum and the papillary muscles. One site in the left ventricular free wall had a significant difference. The signal intensity of the affected myocardium is less than that of the unaffected myocardium. The following table reports the power of each of the sites and the corresponding power using the method described in the analysis subsection (FDR). An (*) indicates those with statistical significance.

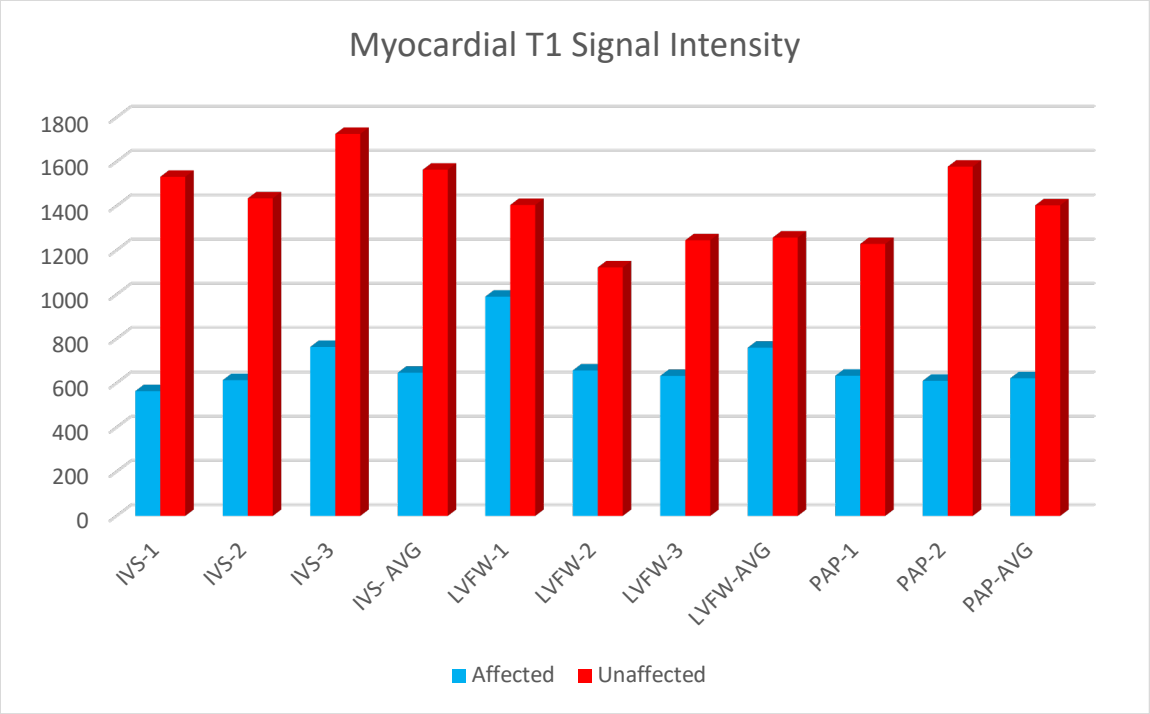

Figure 15. Graph of T1 signal intensity values. Affected in blue, unaffected in red.

Table 10. Cardiovascular T1 signal intensity

Site	Mean (Affected/Unaffected)	Standard Deviation (Affected/Unaffected)	Power (rounded to 0.00)
IVS-1	564.0/1532.0	339.2/393.0	0.006*
IVS-2	613.6/1434.7	238.1/727.7	0.011*
IVS-3	763.6/1725.6	184.7/606.8	0.006*
IVS- AVG	647.1/1564.1	186.2/563.6	0.006*
LVFW-1	990.7/1404.7	358.3/775.1	0.124
LVFW-2	657.4/1122.8	188.2/590.3	0.096
LVFW-3	632.8/1245.4	139.8/234.3	0.045*
LVFW-AVG	760.3/1257.6	151.6/524.5	0.084
PAP-1	633.4/1228.8	70.6/374.6	0.045*
PAP-2	610.6/1577.7	209.4/406.5	0.006*
PAP-AVG	622.0/1403.3	81.7/331.7	0.013*

Similarly, for T1 weighted images with a TE of 1.3 ms, there was sufficient statistical evidence to reject the null hypotheses for those measured points of the interventricular

septum, left ventricular free wall and the papillary muscles. The signal intensity of the affected myocardium is less than that of the unaffected myocardium. The following table reports the power of each of the sites.

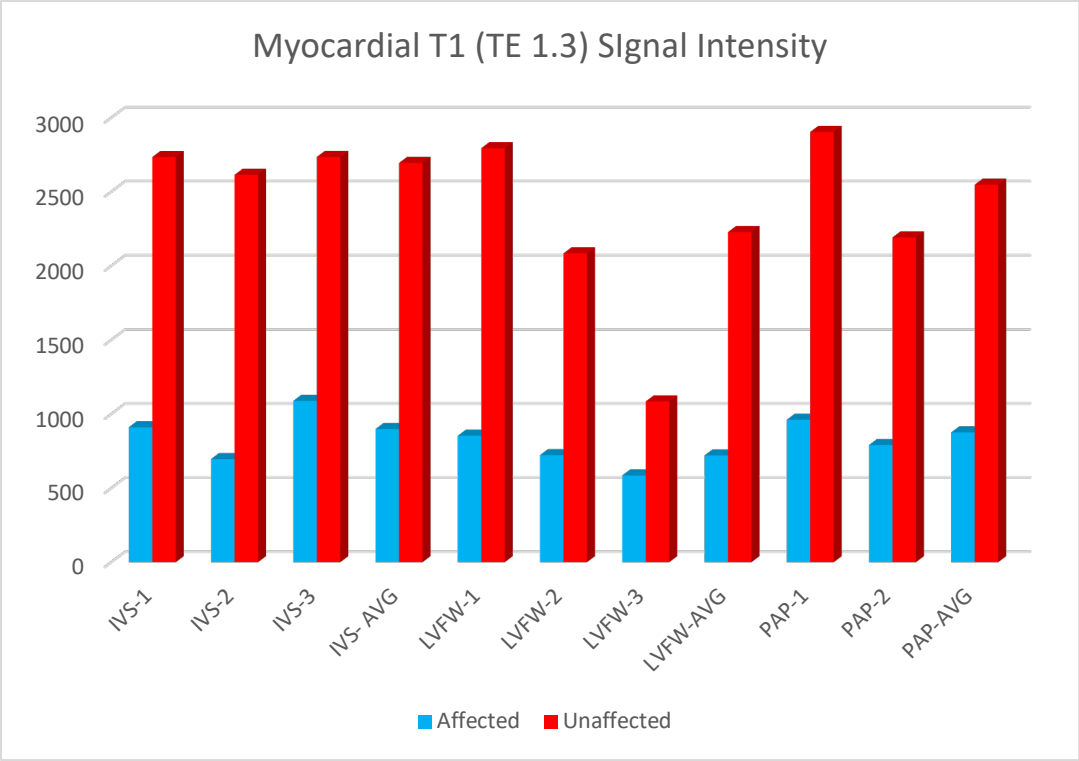

Figure 16. Graph of T1 (TE 1.3) signal intensity values. Affected in blue, unaffected in red.

Table 11. Cardiovascular T1 (TE 1.3) signal intensity

Site	Mean (Affected/Unaffected)	Standard Deviation (Affected/Unaffected)	Power (rounded to 0.00)
IVS-1	911.4/2735.1	440.8/624.9	0.022*
IVS-2	696.4/2615.0	603.2/698.3	0.022*
IVS-3	1089.2/2735.6	800.7/844.3	0.023*
IVS- AVG	899.0/2695.2	571.9/722.5	0.022*
LVFW-1	853.6/2795.0	540.9/868.6	0.022*
LVFW-2	723.0/2085.0	614.3/247.5	0.035*
LVFW-3	585.9/1085.6	565.1/402.5	0.048*
LVFW-AVG	720.9/2228.5	517.2/506.2	0.029*
PAP-1	961.5/2904.5	659.9/699.3	0.022*
PAP-2	791.2/2192.6	577.1/498.4	0.035*
PAP-AVG	876.4/2548.6	609.5/598.8	0.023*

In contrast, for T1 weighted images with a TE of 1.9 ms, there was not sufficient statistical evidence to reject the null hypotheses for those measured points of the interventricular septum, left ventricular free wall and the papillary muscles. The following table reports the power of each of the sites.

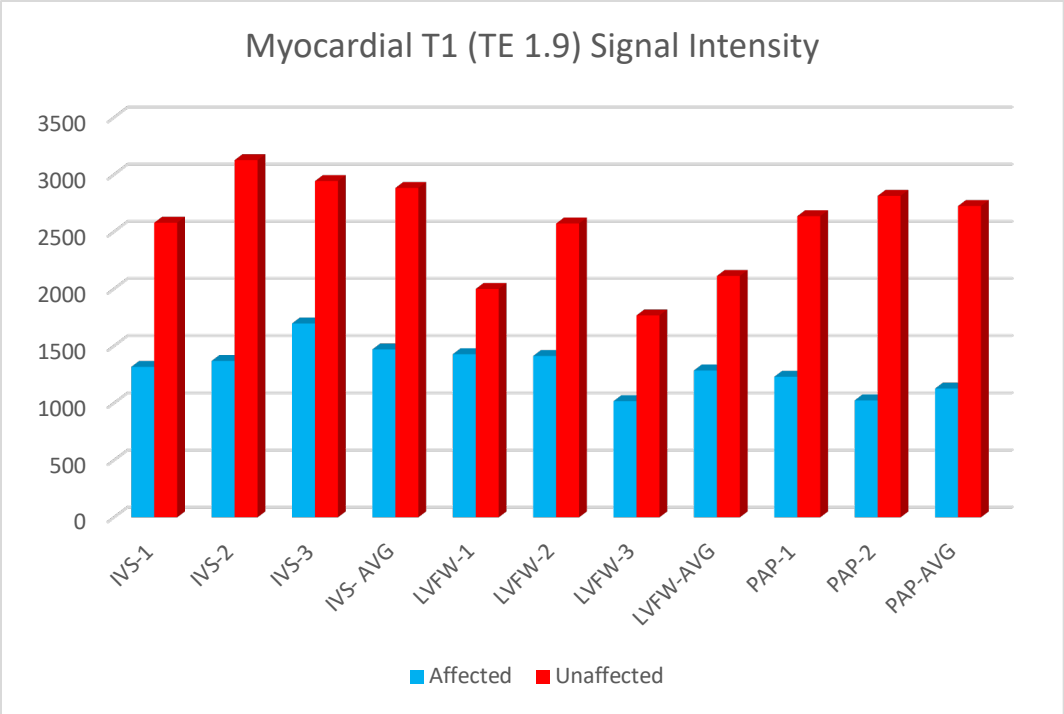

Figure 17. Graph of T1 (TE 1.9) signal intensity values. Affected in blue, unaffected in red.

Table 12. Cardiovascular T1 (TE 1.9) signal intensity

Site	Mean (Affected/Unaffected)	Standard Deviation (Affected/Unaffected)	Power (rounded to 0.00)
IVS-1	1317.1/2579.1	1338.0/1181.0	0.472
IVS-2	1369.2/3126.9	1110.6/896.8	0.472
IVS-3	1696.9/2943.7	930.9/1113.6	0.472
IVS- AVG	1470.1/2883.2	1117.6/1063.8	0.472
LVFW-1	1428.1/1999.7	1356.7/1505.6	0.631
LVFW-2	1412.6/2572.3	1047.6/717.7	0.472
LVFW-3	1017.3/1768.0	1293.6/248.5	0.584
LVFW-AVG	1286.0/2113.3	1188.7/658.2	0.584
PAP-1	1230.8/2636.3	1923.8/1231.7	0.472
PAP-2	1024.1/2814.2	994.3/1300.7	0.472
PAP-AVG	1127.4/2725.3	1448.2/1266.2	0.472

4. Discussion

The results of this study are generally consistent with reported findings in literature and expectations based on the pathophysiology of Duchenne Muscular Dystrophy. In this section, the findings will be considered in sub categories within the data collected from musculoskeletal images and from cardiac images.

4.1 Musculoskeletal

Signal Intensity

A statistical difference was not identified between the signal intensity of the semimembranosus of the affected and the semimembranosus of the unaffected. The expectation based on the pathological progression is that there would be a difference. Although no statistically significant difference was identified, the values between the two populations were noticeably different. The range of values measured in the affected population was 577.2 to 649.7 while the range measured in the unaffected population was 287.4 to 364.7. This result is attributed to the low numbers of subjects presented in this study. The number needed that would be expected to produce a statistically significant difference is 30 animals.

Additionally, the signal intensity of the semimembranosus muscle was compared to the cranial and caudal fascicles of the Sartorius. These muscles were identified in humans as commonly affected and spared, respectively. That is not necessarily observed in this colony

of dogs and therefore, the absence of a statistical difference between signal intensity is an expected result.

Muscle size

The muscle size, reported by ratios to the bone, did not yield a statistically significant difference between the affected and unaffected dogs. It has been reported in both people and dogs that there is an absence of significant difference between affected and unaffected muscles. This is attributed to the deposition of fat both internal to the muscle and between the muscles (20). The internal deposition is attributed to cell death, subsequent inflammation and eventual replacement by fat. Thus, the overall muscle size does not change, just the composition. Early in the manifestations of disease, the calf muscles are visibly enlarged secondary to inflammation. Marden notes that the deposition of fat between muscles occurs "even before intramuscular fatty infiltration is evident" (20). The results reported here are consistently with these findings.

Spectroscopy

The peaks observed between 0.9 and 1.3 ppm correspond to lipid peaks in this non-invasive chemical characterization of the gastrocnemius muscle. Lactate is also resonant at 1.3 ppm. The statistically significant differences were observed at peaks of 0.9 and 1.1 ppm. This result is expected even in early stages of disease as the secondary response of muscle shearing is fat infiltration. As this investigative group continues to explore the longitudinal manifestations of disease, it is expected that spectroscopy will provide diagnostic value in the characterization of muscle composition. Other methods, such as area-under-the-curve, can also be used to characterize each peak and will be considered in future evaluations. Lott et al

describe that separation of intramyocellular lipid at 1.3 ppm and extramyocellular lipid at 1.5ppm is challenging with extensive fat infiltration (31). Younger subjects may offer the opportunity to characterize the process more discretely using this method.

Presently, multi-voxel spectroscopy has the advantage of sampling multiple areas simultaneously and evaluating the variation in pathological manifestation that may exist between different regions of the muscle. While this technique was considered for this study, the limited voxel size and the prolonged time of acquisition were considered sufficiently disadvantageous in comparison to a larger single voxel. The single voxel technique provided a large area which could sufficiently characterize the changes occurring in the muscle belly. As a commonly affected muscle in humans, the head of the gastrocnemius was considered an optimal site. Future spectroscopic investigations will expand to include the antebrachial flexor muscles which are known to be affected commonly in dogs affected by DMD.

The culmination of these results is an elegant example of the characterization of skeletal muscle from the microscopic chemical environment to gross disease. Initial, shear trauma of the myocytes by normal activity results in myocyte death, tissue necrosis and ultimately, fat replacement. During necrosis, an increase in lactate secondary to predominant anaerobic metabolism is expected. Initial fat replacement is expected to be both intra and extra myocellular. Once fat replacement reaches a critical level, the ability to separate intra- from extramyocellular fat is not possible. One would expect the chemical environment to be altered first and most significantly, followed by an intermediate method to assess muscle composition. The gross changes occurring in the muscle (ratio) would be the least sensitive method to characterize the disease state.

4.2 Cardiovascular

Signal Intensity

In the T2 weighted sequence, there was not a statistically significant difference between the signal intensity of the affected myocardium in comparison to the unaffected. While this result is not wholly unexpected since fibrosis has short T2 times and would be similarly hypointense as muscle, there is an observed trend in the data collected. The signal intensity of the affected dogs (range 287.1 to 549.6) was lower than that of the unaffected dogs (range of 577.4 to 934.4). The narrow proximity of the higher values of the affected and lower value of the unaffected could not substantiate a statistical difference with so few subjects. With expansion of the investigated population to increase the number of animals, a significant relationship may be revealed despite the narrow margin between groups.

The T1 weighted images were performed with three different time of echo during the development of the protocol and each was considered separately. The T1 weighted images had a statistically significant difference in the signal intensity of the affected myocardium from the unaffected myocardium in the interventricular septum and the papillary muscles. T1 weighted images performed with a TE of 1.3 ms identified significant differences between the affected and unaffected groups at all locations. T1 weighted images using a TE of 1.9 ms did not yield a significant difference in signal intensity between the affected and unaffected group. Although the specific reason for this finding is unknown, current techniques in cardiac MR employ ultrashort TE, however, both TE 1.3 ms and 1.9 ms are useful in the characterization. The author has most commonly identified a 1.9 ms TE in association with 3D imaging; in this study it was applied to a two-plane technique. The

difference between these two groups is consistent with described pathology in the myocardium with disease progression as lower signal intensity is associated with fibrosis that would occur in affected myocardium.

Bilchick et al described greater scar formation in the free wall over the septal segments in people in the mid cavity and at the base (39). In dogs, Kornegay et al sites that they have fibrosis distributed in the left ventricular papillary muscle and free wall at the apex (18). The reasons for this distribution pattern are unknown but their recognition is vital to future gene therapy interventions that may be administered by direct inoculation. It can be postulated that this may be due to the greater range of motion in the mid chamber and base, resulting in more myocardial myocyte trauma through these levels; ultimately shear damage would lead to replacement by fibrosis. Kornegay et al note the presence of mineralization as well on histopathologic evaluation of these areas (18). Characterization was strengthened using late gadolinium enhancement in a preliminary study the Kornegay group performed with a different population of dogs.

4.3 Limitations and Future Directions

The major limitation of this study is the small number of subjects. It undermines the strength of the relationships described. However, the recognized trends in such a small number of subjects is encouraging as this study will expand to other age groups and carrier dogs. Additionally, delayed gadolinium enhancement will be evaluated as well as spectroscopy in the myocardium. Delayed gadolinium enhancement is most commonly used to assess for the presence of fibrosis with the delayed wash in and delayed wash out

effect that arises from diminished yet minimally preserved perfusion to this tissue. The culmination of this effort will be a firm foundation from which to characterize the efficacy of novel therapies. Duan et al have pursued musculoskeletal gene therapies with initial success in dogs while myocardial gene therapies have been explored only in the *mdx* mouse model (47). Spectroscopy may provide a critical means to evaluate the early success in therapies as the chemical environment of the cell can be repeatedly "sampled" without the trauma of biopsy.

A minor, but necessary, limitation in this study is the use of anesthesia for completion of the MRI study. Anesthesia is known to alter cardiac dynamics, thus impairing use of strain analysis in these subjects. In the anesthetic protocol employed here, dexmedetomidine can cause decreased cardiac output although the mechanism is unknown (48). Murrell proposes that this may be associated with the increased afterload by increased systemic vascular resistance (48). Propofol has been demonstrated to decrease the right ventricular ejection fraction and the end systolic volume index in mice (49). Early cardiac disease is recognized by diastolic dysfunction while later manifestations affect the systolic function of the myocardium. Myocardial strain analysis with MRI has been at the forefront of early recognition of cardiac dysfunction in people. The medications used in this protocol prohibit our ability to quantify changes in strain, thus preventing characterization of early myocardial changes.

Given the importance of strain analysis in cardiac magnetic resonance evaluation, methods to circumvent this limitation could include simultaneous evaluation by pre and immediately post- anesthetic induction echocardiograms. However, the use of normal and carrier control

populations may be sufficient to establish a relationship. Ameen et al note that the "contraction speed and the force are significantly altered in the atria even in young [affected] mice and this is found before there is any obvious necrosis and resulting fibrosis of the walls of the ventricles of the heart" (6). The group suggests that altered function in the membrane ion channels regulating calcium are more significant than the fibrosis or cell death. Thus, the differences between the affected, carrier and normal populations could describe the alteration in function.

In spite of the limitations of this study, noteworthy differences are acknowledged between the affected and unaffected populations in advanced stages of disease. Sequences deemed most valuable for future investigations should include T2 weighted sequences and spectroscopy for musculoskeletal assessment and T1 weighted sequences for myocardial evaluation. Additional sequences that should be incorporated in the future of myocardial evaluation include T1 post gadolinium administration for delayed enhancement and spectroscopy of the interventricular septum and papillary muscle. It is expected that these relationships will become more strongly and discretely defined as this work continues with more dogs and different age groups. The aim of this work is to provide a foundation from which assessment of therapies can be non-invasively monitored and measured. The marked differences present in spectroscopic evaluation may provide the ability to assess the earliest micro-environmental changes in muscle for this purpose. This body of work is suggestive that this is feasible.

Bibliography:

1. Emery, A. E., Muntoni, F., & Quinlivan, R. C. (2015). *Duchenne muscular dystrophy*. OUP Oxford.

2. Sussman, M. (2002). Duchenne muscular dystrophy. *JAAOS-Journal of the American Academy of Orthopaedic Surgeons*, *10*(2), 138-151.

3. Kuhn, E. (1990). From dystrophia muscularis progressiva to dystrophin.

4. Yiu, E. M., & Kornberg, A. J. (2015). Duchenne muscular dystrophy. *Journal of paediatrics and child health*, *51*(8), 759-764.

5. Nowak, K. J., & Davies, K. E. (2004). Duchenne muscular dystrophy and dystrophin: pathogenesis and opportunities for treatment. *EMBO reports*, *5*(9), 872-876.

6. Ameen, V., & Robson, L. G. (2010). Experimental models of duchenne muscular dystrophy: relationship with cardiovascular disease. *The open cardiovascular medicine journal*, *4*, 265.

7. Spurney, C. F. (2011). Cardiomyopathy of Duchenne muscular dystrophy: current understanding and future directions. *Muscle & nerve*, *44*(1), 8-19.

8. Bushby, K., Finkel, R., Birnkrant, D. J., Case, L. E., Clemens, P. R., Cripe, L., ... & DMD Care Considerations Working Group. (2010). Diagnosis and management of Duchenne muscular dystrophy, part 1: diagnosis, and pharmacological and psychosocial management. *The Lancet Neurology*, *9*(1), 77-93.

9. Mirski, K. T., & Crawford, T. O. (2014). Motor and cognitive delay in Duchenne muscular dystrophy: implication for early diagnosis. *The Journal of pediatrics*, *165*(5), 1008-1010.

10. Birnkrant, D. J., Bushby, K., Bann, C. M., Alman, B. A., Apkon, S. D., Blackwell, A., ... & Sheehan, D. W. (2018). Diagnosis and management of Duchenne muscular dystrophy, part 2: respiratory, cardiac, bone health, and orthopaedic management. *The Lancet Neurology*.

11. Guglieri, M., & Bushby, K. (2015). Recent developments in the management of Duchenne muscular dystrophy. *Paediatrics and Child Health*, *25*(11), 505-514.

12. Duan, D. (2006). Challenges and opportunities in dystrophin-deficient cardiomyopathy gene therapy. *Human molecular genetics*, *15*(suppl 2), R253-R261.

13. Birnkrant, D. J., Bushby, K., Bann, C. M., Apkon, S. D., Blackwell, A., Colvin, M. K., ... & Naprawa, J. (2018). Diagnosis and management of Duchenne muscular dystrophy, part 3: primary care, emergency management, psychosocial care, and transitions of care across the lifespan. *The Lancet Neurology*.

14. Papa, R., Madia, F., Bartolomeo, D., Trucco, F., Pedemonte, M., Traverso, M., ... & Fiorillo, C. (2016). Genetic and early clinical manifestations of females heterozygous for Duchenne/Becker muscular dystrophy. *Pediatric neurology*, *55*, 58-63.

15. Finsterer, J., & Stollberger, C. (2018). Muscle, cardiac, and cerebral manifestations in female carriers of dystrophin variants. *Journal of the Neurological Sciences*.

16. Hoogerwaard, E. M., Van der Wouw, P. A., Wilde, A. A. M., Bakker, E., Ippel, P. F., Oosterwijk, J. C., ... & de Visser, M. (1999). Cardiac involvement in carriers of Duchenne and Becker muscular dystrophy. *Neuromuscular Disorders*, *9*(5), 347-351.

17. Valentine, B. A., Winand, N. J., Pradhan, D., Moise, N., de Lahunta, A., Kornegay, J. N., & Cooper, B. J. (1992). Canine X-linked muscular dystrophy as an animal model of Duchenne muscular dystrophy: A review. *American Journal of Medical Genetics Part A*, *42*(3), 352-356.

18. Kornegay, J. N., Bogan, J. R., Bogan, D. J., Childers, M. K., Li, J., Nghiem, P., ... & Tou, S. (2012). Canine models of Duchenne muscular dystrophy and their use in therapeutic strategies. *Mammalian genome*, *23*(1-2), 85-108.

19. Howell, J. M., Fletcher, S., Kakulas, B. A., O'hara, M., Lochmuller, H., & Karpati, G. (1997). Use of the dog model for Duchenne muscular dystrophy in gene therapy trials. *Neuromuscular Disorders*, *7*(5), 325-328.

20. Marden, F. A., Connolly, A. M., Siegel, M. J., & Rubin, D. A. (2005). Compositional analysis of muscle in boys with Duchenne muscular dystrophy using MR imaging. *Skeletal radiology*, *34*(3), 140-148.

21. Thibaud, J. L., Azzabou, N., Barthelemy, I., Fleury, S., Cabrol, L., Blot, S., & Carlier, P. G. (2012). Comprehensive longitudinal characterization of canine muscular dystrophy by serial NMR imaging of GRMD dogs. *Neuromuscular Disorders*, *22*, S85-S99

22. Thibaud, J. L., Monnet, A., Bertoldi, D., Barthelemy, I., Blot, S., & Carlier, P. G. (2007). Characterization of dystrophic muscle in golden retriever muscular dystrophy dogs by nuclear magnetic resonance imaging. *Neuromuscular disorders*, *17*(7), 575-584.

23. Mercuri, E., Pichiecchio, A., Allsop, J., Messina, S., Pane, M., & Muntoni, F. (2007). Muscle MRI in inherited neuromuscular disorders: past, present, and future. *Journal of Magnetic Resonance Imaging*, *25*(2), 433-440.

24. Matsumura, K., Nakano, I., Fukuda, N., Ikehira, H., Tateno, Y., & Aoki, Y. (1988). Protron spin-lattice relaxation time of duchenne dystrophy skeletal muscle by magnetic resonance imaging. *Muscle & nerve*, *11*(2), 97-102.

25. Finanger, E. L., Russman, B., Forbes, S. C., Rooney, W. D., Walter, G. A., & Vandenborne, K. (2012). Use of skeletal muscle MRI in diagnosis and monitoring disease

progression in Duchenne muscular dystrophy. *Physical medicine and rehabilitation clinics of North America*, *23*(1), 1-10.

26. Garrood, P., Hollingsworth, K. G., Eagle, M., Aribisala, B. S., Birchall, D., Bushby, K., & Straub, V. (2009). MR imaging in duchenne muscular dystrophy: quantification of T1-weighted signal, contrast uptake, and the effects of exercise. *Journal of Magnetic Resonance Imaging*, *30*(5), 1130-1138.

27. Kobayashi, M., Nakamura, A., Hasegawa, D., Fujita, M., Orima, H., & Takeda, S. I. (2009). Evaluation of dystrophic dog pathology by fat-suppressed T2-weighted imaging. *Muscle & nerve*, *40*(5), 815-826.

28. Kim, H. K., Laor, T., Horn, P. S., Racadio, J. M., Wong, B., & Dardzinski, B. J. (2010). T2 mapping in Duchenne muscular dystrophy: distribution of disease activity and correlation with clinical assessments. *Radiology*, *255*(3), 899-908.

29. Mathur, S., Lott, D. J., Senesac, C., Germain, S. A., Vohra, R. S., Sweeney, H. L., ... & Vandenborne, K. (2010). Age-related differences in lower-limb muscle cross-sectional area and torque production in boys with Duchenne muscular dystrophy. *Archives of physical medicine and rehabilitation*, *91*(7), 1051-1058.

30. Aisen, A. M., & Chenevert, T. L. (1989). MR spectroscopy: clinical perspective. *Radiology*, *173*(3), 593-599.

31. Lott, D. J., Forbes, S. C., Mathur, S., Germain, S. A., Senesac, C. R., Sweeney, H. L., ... & Vandenborne, K. (2014). Assessment of intramuscular lipid and metabolites of the lower leg using magnetic resonance spectroscopy in boys with Duchenne muscular dystrophy. *Neuromuscular Disorders*, *24*(7), 574-582.

32. Kinali, M., Arechavala-Gomeza, V., Cirak, S., Glover, A., Guglieri, M., Feng, L., ... & Quinlivan, R. M. (2011). Muscle histology vs MRI in Duchenne muscular dystrophy. *Neurology*, *76*(4), 346-353.

33. Klingler, W., Jurkat-Rott, K., Lehmann-Horn, F., & Schleip, R. (2012). The role of fibrosis in Duchenne muscular dystrophy. *Acta Myologica*, *31*(3), 184.

34. Ringleb, S. I., Bensamoun, S. F., Chen, Q., Manduca, A., An, K. N., & Ehman, R. L. (2007). Applications of magnetic resonance elastography to healthy and pathologic skeletal muscle. *Journal of Magnetic Resonance Imaging*, *25*(2), 301-309.

35. Silva, M. C., Meira, Z. M. A., Giannetti, J. G., da Silva, M. M., Campos, A. F. O., de Melo Barbosa, M., ... & Rochitte, C. E. (2007). Myocardial delayed enhancement by magnetic resonance imaging in patients with muscular dystrophy. *Journal of the American College of Cardiology*, *49*(18), 1874-1879.

36. Mou, Y. A., Lacampagne, A., Irving, T., Scheuermann, V., Blot, S., Ghaleh, B., ... & Cazorla, O. (2018). Altered myofilament structure and function in dogs with Duchenne muscular dystrophy cardiomyopathy. *Journal of molecular and cellular cardiology*, *114*, 345-353.

37. Forder, J. R., & Pohost, G. M. (2003). Cardiovascular nuclear magnetic resonance: basic and clinical applications. *The Journal of clinical investigation*, *111*(11), 1630-1639.

38. Kellman, P., Hernando, D., & Arai, A. E. (2010). Myocardial fat imaging. *Current cardiovascular imaging reports*, *3*(2), 83-91.

39. Bilchick, K. C., Salerno, M., Plitt, D., Dori, Y., Crawford, T. O., Drachman, D., & Thompson, W. R. (2011). Prevalence and distribution of regional scar in dysfunctional myocardial segments in Duchenne muscular dystrophy. *Journal of Cardiovascular Magnetic Resonance*, *13*(1), 20.

40. Kimura, T., Ikedo, M., & Takemoto, S. (2011). Phase enhancement for time-of-flight and flow-sensitive black-blood MR angiography. *Magnetic resonance in medicine*, *66*(2), 437-447.

41. D'angelo, M. G., Gandossini, S., Boneschi, F. M., Sciorati, C., Bonato, S., Brighina, E., ... & Brunelli, S. (2012). Nitric oxide donor and non steroidal anti inflammatory drugs as a therapy for muscular dystrophies: evidence from a safety study with pilot efficacy measures in adult dystrophic patients. *Pharmacological research*, *65*(4), 472-479.

42. Thomas, G. D., Ye, J., De Nardi, C., Monopoli, A., Ongini, E., & Victor, R. G. (2012). Treatment with a nitric oxide-donating NSAID alleviates functional muscle ischemia in the mouse model of Duchenne muscular dystrophy. *PLoS One*, *7*(11), e49350.

43. Dudley, R. W., Lu, Y., Gilbert, R., Matecki, S., Nalbantoglu, J., Petrof, B. J., & Karpati, G. (2004). Sustained improvement of muscle function one year after full-length dystrophin gene transfer into mdx mice by a gutted helper-dependent adenoviral vector. *Human gene therapy*, *15*(2), 145-156.

44. Nance, M. E., Hakim, C. H., Yang, N. N., & Duan, D. (2018). Nanotherapy for Duchenne muscular dystrophy. *Wiley Interdisciplinary Reviews: Nanomedicine and Nanobiotechnology*, *10*(2).

45. Ichim, T. E., Alexandrescu, D. T., Solano, F., Lara, F., Campion, R. D. N., Paris, E., ... & Marleau, A. M. (2010). Mesenchymal stem cells as anti-inflammatories: implications for treatment of Duchenne muscular dystrophy. *Cellular immunology*, *260*(2), 75-82.

46. Barnard, A. M., Willcocks, R. J., Finanger, E. L., Daniels, M. J., Triplett, W. T., Rooney, W. D., ... & Harrington, A. T. (2018). Skeletal muscle magnetic resonance biomarkers correlate with function and sentinel events in Duchenne muscular dystrophy. *PloS one*, *13*(3), e0194283.

47. McGreevy, J. W., Hakim, C. H., McIntosh, M. A., & Duan, D. (2015). Animal models of Duchenne muscular dystrophy: from basic mechanisms to gene therapy. *Disease models & mechanisms*, *8*(3), 195-213.

48. Murrell, J. C., & Hellebrekers, L. J. (2005). Medetomidine and dexmedetomidine: a review of cardiovascular effects and antinociceptive properties in the dog. *Veterinary anaesthesia and analgesia*, *32*(3), 117-127.

49. Kellow, N. H., Scott, A. D., White, S. A., & Feneck, R. O. (1995). Comparison of the effects of propofol and isoflurane anaesthesia on right ventricular function and shunt fraction during thoracic surgery. *British journal of anaesthesia*, *75*(5), 578-582.